Astronomical adaptive optics.
II. Experimental results of an optimized modal control[*]

E. Gendron[1,2] and P. Léna[1]

[1] Observatoire de Paris et Université Paris VII, U.R.A. CNRS 264, F-92195 Meudon Cedex, France
[2] Laserdot, Route de Nozay, F-91460 Marcoussis, France

Abstract. — A previous paper discussed the possible improvement of the image quality given by an adaptive optics (AO) system by optimizing its spatial and temporal correction performance. Considering the perturbed wavefront as a weighted sum of spatial modes, this optimization leads us to attribute a specific correction bandwidth to each mode, depending on its signal to noise ratio and correlation time. These parameters are related to the particular observation being carried out as they depend on the magnitude, colour and extension of the reference source, on the seeing conditions and on the system characteristics. In this article these considerations are verified on the basis of experimental data provided by the wave-front analyser of the AO system ComeOnPlus. Algorithms to process the wavefront data are described and their performance and robustness are discussed. The results are analysed and the efficiency of the AO system is derived in terms of the reference source magnitude and atmospheric conditions.

1. Introduction

In a previous theoretical paper (Gendron & Léna 1994a), hereafter Paper I, the optimization of modal control applied to an astronomical adaptive optics (AO) system was described.

Such optimization aims to adapt various parameters of the system (number of degrees of freedom or modes, temporal response, gains of the loop) to the observing conditions (e.g. magnitude of the reference source, intensity and speed of turbulence) in order to minimize the residual phase error. This error is directly linked to the image Strehl ratio at small values, but beyond a value of 1 rd^2 the image quality becomes a more complex function of it. We however choose this criterium since in any case the flatter the wavefront, the better is the image (Hermann 1992). Moreover, the phase minimization criterion is well suited for modal analysis.

The principle of modal optimization, as described in our Paper I and experimentally demonstrated here, is independently proposed in a recent theoretical paper (Ellerbroek et al. 1994). These authors choose to optimize jointly the modes and the correction bandwidths, while in our approach the modes are selected beforehand to best fit

the atmospheric conditions and then the correction bandwidth for each mode is optimized.

The particular AO system ComeOnPlus (Gendron et al. 1991; Hubin et al. 1992; Rousset et al. 1993; Rousset et al. 1994), extensively operated on the 3.6 m telescope at La Silla (Chile) between 1992 and 1994 is briefly described in Sect. 3. It provided a wealth of experimental data covering a wide range of observing conditions.

In Sect. 4 a variety of system behaviours related to various turbulence states of the atmosphere is described. Since a key issue in modal optimization is related to the noise introduced in the wavefront measurements made by the wavefront sensor (WFS), several methods for evaluating this contribution are presented in Sect. 5.

In Sect. 7, the effectiveness of the optimization scheme, as described in Paper I, is analysed for various observing conditions encountered during a number of astronomical runs.

2. Notation

For consistency with the previous paper, the notation used throughout this paper is summarized in Table 1.

Table 1. Notation

Quantity	Signification
f	frequency
t	time
F_e	sampling frequency
T_e	sampling period $(1/F_e)$
τ	time delay between measurement and control
$h_{wfs}(f)$	transfer function of the WFS
$h_{sys}(f)$	transfer function of the rest of the system
$h_{ol}(f)$	open loop transfer function
g_i	modal gain number i
$r_0(\lambda)$	Fried's parameter at wavelength λ
L_0	outer scale of the turbulence
τ_0	correlation time
H_{cor}	square modulus of the system correction transfer function
H_n	square modulus of the transfer function between the noise input and the noise sent on the mirror mode controls
$T(f)$	spectra of the mode coefficient fluctuations due to the atmospheric turbulence
$B(f)$	spectra (white) of the mode coefficient fluctuations due to the noise
b_0	level of $B(f)$
b	(wrong) estimation of b_0
$-u$	exponent of the asymptotic behavior of $T(f)$ at high frequency $(T(f) \propto f^{-u})$
ν	correction bandwidth
ν_0	optimum correction bandwidth
ν_w	wrong optimum correction bandwidth
$\epsilon(\nu)$	calculated residual phase error on a mode versus correction bandwidth
$\epsilon_0(\nu)$	actual residual phase error on a mode versus correction bandwidth

3. The adaptive optics system ComeOnPlus

3.1. The instrument

The AO system ComeOnPlus is installed on the ESO 3.6 m telescope of La Silla (Chile). It is equipped with a piezostack type deformable mirror with 8 × 8 actuators forming a regular grid on the pupil. Only 52 of the actuators are used. Figure 1 shows the geometry of the actuators.

Two Shack-Hartmann type WFS are available on the optical bench. The first is dedicated to high flux reference sources (visual magnitude $m_V \lesssim 10$). It is based on a 100 × 100 intensified Reticon photodiode array, with a sampling rate of 200 Hz. The second one, dedicated to fainter references ($m_V \gtrsim 10$), is an Electron-Bombarded CCD (EBCCD) (Cuby et al. 1990) acting as a photon-counting device. This detector functions like a first generation intensifier tube, with a thinned back-side bombarded CCD in place of the classic phosphor screen. Its main advantages are the total lack of remanence and dispersion
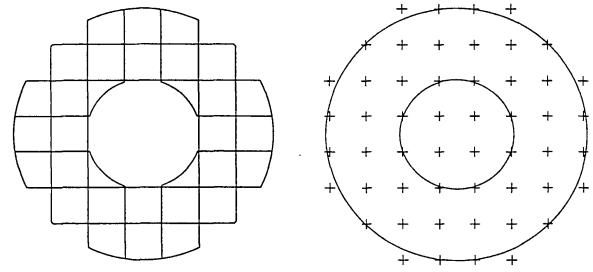

Fig. 1. Wavefront sensor (left) and mirror (right) geometry of the ComeOnPlus AO system. The crosses stand for the actuator position

of the intensification gain. The value of the latter can be set between 1800 and 2000 depending on the high voltage. The sampling frequency is adjustable from 25 to 200 Hz whithout modifying the read-out time. Both WFS have 7 × 7 subapertures. Only 32 subapertures out of 49 are useful, providing 64 independent slope measurements on the wavefront. The geometry is shown in Fig. 1. The diameter of the pupil is 3.6 m with a central obscuration of 1.57 m.

3.2. The control loop

The control algorithm of ComeOnPlus consists of an integral compensator. Although the AO system discretizes the temporal signals, only continuous signals will be considered here, since the correction bandwidth remains small compared to the sampling frequency. Hence the transfer function due to the temporal filtering of the detector can be written

$$h_{wfs}(f) = \text{sinc}(\pi f T_e).e^{-i\pi f T_e} \qquad (1)$$

The transfer function formed by the integral compensator, the modal gain g_i and by the time delay τ is

$$h_{sys}(f, g_i) = g_i.\frac{F_e\, e^{-2i\pi\tau f}}{2i\pi f} \qquad (2)$$

The product of those functions form the open-loop transfer function $h_{ol}(f, g_i) = h_{wfs}(f).h_{sys}(f, g_i)$. We define the rejection transfer function (here called correction transfer function) as

$$H_{cor}(f, g_i) = \left|\frac{1}{1 + h_{ol}(f, g_i)}\right|^2 \qquad (3)$$

and the transfer function between the white noise at input and the noise output on the mirror mode controls

$$H_n(f, g_i) = \left|\frac{h_{sys}(f, g_i)}{1 + h_{ol}(f, g_i)}\right|^2 \qquad (4)$$

3.3. The data

When running, the system provides two sets of data. Images of the source which are weakly time dependent (Rigaut et al. 1991), and the data flowing from the wavefront computer. This paper primarily considers the latter. They consist of the two coordinates for each of the 32 spots of the WFS. At each sampling period this vector of 64 components is computed and stored. As this quantity represents the local wavefront slopes at each subaperture, it is called a *slope frame*. A set of slope frames is called a *slope set*. This terminology will be used below. Data can be recorded while the loop is either closed or open. The number of frames in a slope set is a power of 2, and all the slope frames it contains are sequential in time, hence there are no missing data. Unfortunately, there are various experimental limitations inherent to the system that affect the quality of the data.

Some examples are illustrated by Figs. 2 and 3. They represent the tilt value versus time. 'Incidents' are visible on these records and come from parasitic discharges in the tube or from mistakes made by the system operator. Such events are common and remain unnoticed unless special action is taken: the slope sets corresponding to Figs. 2 and 3 can go through the whole modal control optimization algorithm as described in Paper I, through r_0 and τ_0 computation or through the noise level computation without giving either aberrant, nor true results. Hence, in order to ensure the reliability of the data, all the slope sets have to be carefully pre-processed through an 'incident detector' and defective slope sets are eliminated.

Fig. 3. Tilt value (units are arcseconds) versus time. A break is clearly visible in the record. It separates a servoed zone from an uncorrected one. This artefact comes from a mistake of the operator

Fig. 4. Trace of the wander of two spots of the SH sensor. The borders represent the limit of the subaperture field. The ticks indicate the pixel borders. On the right, an example of a normal behavior. On the left, the abnormal behavior is produced by a spot entering in the zone reserved to another
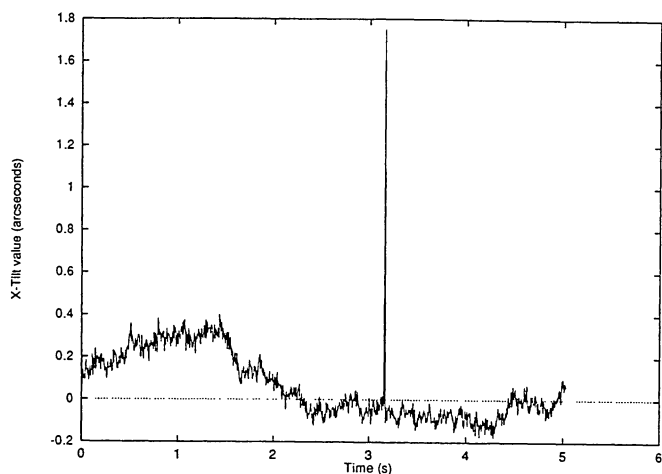

Fig. 2. Tilt value (units are arcseconds) versus time. The artefact may come from a ion surge or a parasitic discharge on the intensifier high-voltage

Another limitation is introduced by the WFS: its field of view has a radius of 3 arcsec, while the telescope pointing accuracy is about 0.5 arcsec. It may happen in open loop that a spot spreads into a detector zone dedicated to
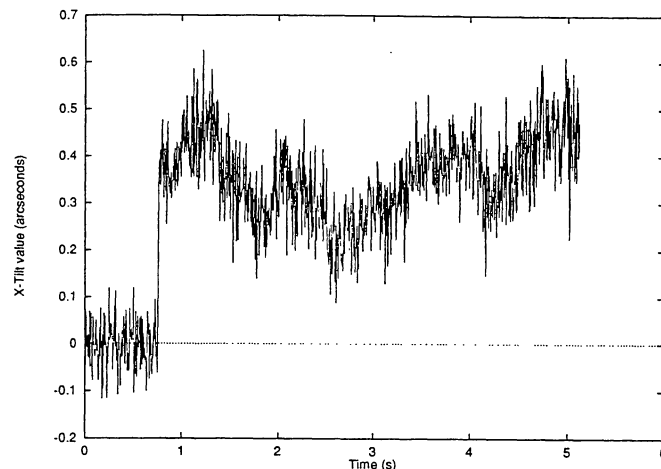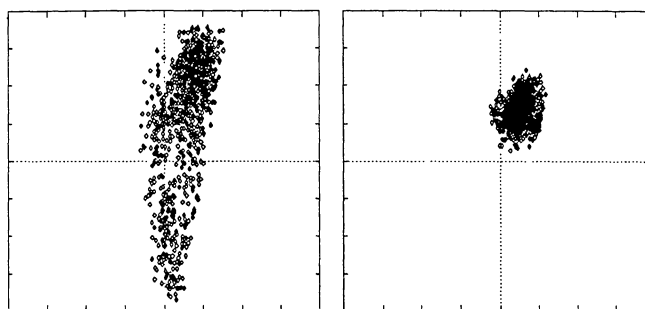
the neighbouring spot, even before reaching the 3 arcsec limit imposed by the field diaphragm. Nothing prevents such an event from happening.

Figure 4 is an illustration of what happens in such a case: this modifies the cross-correlation between the centroid fluctuations, leading to a biased estimate of the modal decomposition of the wavefront. In order to avoid this problem, open loop data may be weakly "tilt-servoed" with a correction bandwidth of about 0.1 Hz. In addition, the telescope aberrations are compensated by applying the adequate static driving voltages on the active mirror.

4. Turbulence structure from experimental data

4.1. General considerations

Many articles dealing with AO system performance assume a particular turbulence model, the Kolmogorov one

beeing extensively used. Unfortunately, the ComeOnPlus measurements have shown that this model is not always applicable. The turbulence structure is sometimes more sophisticated. The local seeing is often significantly non-Kolmogorov. This term encapsulates all the wavefront perturbations occuring near the telescope: the dome seeing, the primary mirror seeing and all the local convective effects. These effects depend on the telescope position, on the temperature difference between inside and outside the dome, and are extremely difficult to predict or model in practice. They are a source of anisotropic perturbations over the pupil. As an example, Fig. 8 shows the variance of the noise value over all the subapertures. As more extensively discussed in Sect. 5.3, it suggests that in some cases, the usual hypothesis upon which some parameters remains uniform over the pupil is incorrect. The variance of the angle of arrival may also be inhomogeneous over the pupil.

These remarks lead one to promogulate whenever possible the direct use of observed quantities to optimize the modal control, rather than a priori models.

4.2. Temporal power spectra and autocorrelations

An important quantity in the power spectral densities of the modes is the behavior at high temporal frequency since it determines the autocorrelation profile near the origin. According to several authors (Madec et al. 1992; Conan et al. 1992; Roddier et al. 1993) this behavior should be in $f^{-17/3}$ for a single turbulent layer, a plane wave, and Kolmogorov-type turbulence. As Madec et al. (1992) state, this behavior has never been observed in data obtained with the ComeOnPlus system. The steepest decrease ever seen is close to $f^{-11/3}$, but this is very difficult to characterize.

The power spectrum is related to the autocorrelation profile via a Fourier transform. The behavior of the autocorrelation $A(t)$ near the origin guess some indication about the high frequency slope value. We want to evaluate $A(0) - A(t)$ near the origin as a series in t. The low-frequency part of the spectrum only contributes to it in t^2, or smoother (t^4, etc). Sharper patterns can only be produced by the high-frequency regime of the spectrum in f^{-u}, which is linked to the autocorrelation $A(t)$ by

$$A(t) = \int f^{-u}.\cos(2\pi ft)\,\mathrm{d}f \qquad (5)$$

When the spectrum drops off faster than f^{-3}, its influence on the autocorrelation profile $A(0)-A(t)$ near the origin is somewhat smoother than t^2 and is then sufficiently steep to be overridden by the low frequencies contribution.

We assume $3 > u > 1$. The integral in Eq. (5) is not defined because of f^{-u} when f tends towards 0. Although incorrect since $A(0)$ does not exist, a way to work around this is to write

$$
\begin{aligned}
A(t) &= A(0) - \int f^{-u}.(1 - \cos(2\pi ft))\,\mathrm{d}f \\
&= A(0) - 2 \int f^{-u}.\sin^2(\pi ft)\,\mathrm{d}f \\
&= A(0) + \frac{(2\pi)^u}{4\,\Gamma(u)\,\cos(u\frac{\pi}{2})}\,|t|^{u-1} \qquad (6)
\end{aligned}
$$

This shows that a high-frequency regime in f^{-u} generally creates an autocorrelation profile in $a|t|^{u-1} + b|t|^2 + o(|t|^3)$, a characterizing the energy contained in the high frequency part, and b in the low frequency part. Hence, the autocorrelation profile is always close to a parabola. This property will be used in Sect. 5.

5. Noise determination

In Paper I, the importance of a proper knowledge of the noise was underlined. The noise comes from the finite number of photocounts received on the WFS detector. It is usually a superposition of photon noise and read-out noise of the detector. We study hereafter the precision of different methods of measuring this noise level.

5.1. Methods to measure the noise

To properly implement the modal control optimization, a reliable method to determine the noise is essential. We compare here the performance of two methods. The first one is described by Gendron & Léna (1994a): it derives the noise from the variance of a special configuration of the slope measurements which is very unlikely to be caused by the atmosphere, but to the contrary most likely to be due to the above mentioned noise sources. This approach, called method (a) below, has the disadvantage of providing only a global noise value averaged over the pupil.

An alternative method was originally proposed by Rousset (1992), and allows one to compute the noise at each subaperture. It uses the fact that since the noise is uncorrelated between successive frames, its time autocorrelation is a Dirac function. Moreover, it is not correlated with the fluctuations caused by the atmosphere (namely the turbulent signal). Hence, the time autocorrelation of the centroid position within one particular subaperture is the sum of the actual turbulent signal autocorrelation plus the noise autocorrelation, since noise and signal are independent. The signal autocorrelation is affected by the noise only at the origin. Hence, a fit of the autocorrelation near the origin by a parabola (see Sect. 4.2) allows one to determine the signal variance without noise contribution (see Fig 5). The noise variance is deduced from the total value at origin, minus the parabola value. This method will be called method (b) hereafter.

It is worth noticing that methods (a) and (b) do not use the same physical principles. Comparing their results
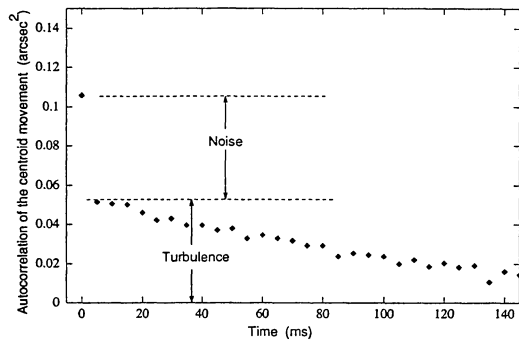
Fig. 5. The autocorrelation of the WFS measurement fluctuations is the sum of the noise autocorrelation (Dirac) and of the actual turbulent wavefront slope autocorrelation. Experimental data. The conditions are $r_0=10.5$ cm, $\tau_0=80$ ms, $F_e=200$ Hz. The average noise over the whole Shack-Hartmann is 0.082 arcsec^2

may be instructive and is the subject of the next paragraph.

5.2. Comparison of methods

As both methods were designed to be adequate on simulated data, their applicability to real data is of interest. In this case, the non-uniformity of the noise sources over the pupil may introduce differences (see Sect. 5.3).

In Fig. 6 is plotted the noise determined with method (a) versus the averaged noise derived with method (b), using 73 slope sets covering five consecutive nights. One notices a weak dispersion near the full correlation straight line.

Making the reasonnable assumption that both methods show independent dispersion as they are based on different principles (one uses temporal properties while the other uses spatial properties of the noise), the squares of the standard deviation may be added and the total dispersion is cumulative of both: hence, the standard deviation of each method is estimated by taking half the value shown in Fig. 6.

Figure 7 shows the result, by plotting the following quantity: logarithm of the ratio of noise variances determined by (a) and (b). This histogram shows a standard deviation of 0.16. Either methods lead to an error in the noise estimate which is therefore 0.11 ($= 0.16/\sqrt{2}$) times the noise variance.

Granted this quantitative equivalence of both methods, method (b) will be preferred to (a) as it reliably gives the noise in each subaperture, and therefore takes into account the various inhomogeneities described above.

Assuming from now on that the method (b) is reliable enough, it is possible to show different properties of the noise variance. This is the subject of Sect. 5.3.
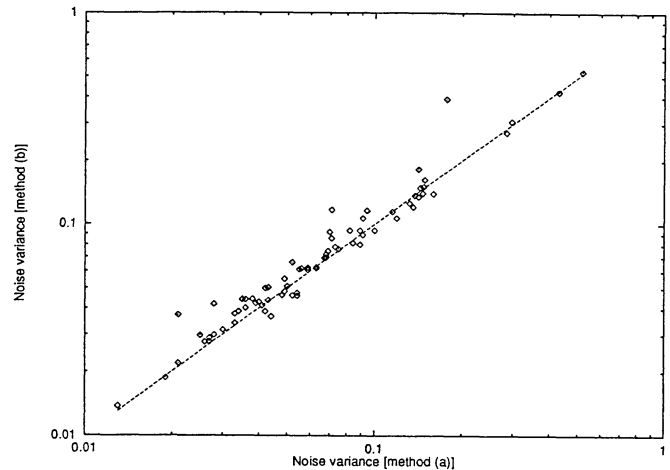

Fig. 6. Variance of the error on the determination of the spot centroid computed with the method (b) in terms of the one obtained with method (a). The straight line represents a full correlation. Since the two methods are based on different principles, the good agreement demonstrates their reliability
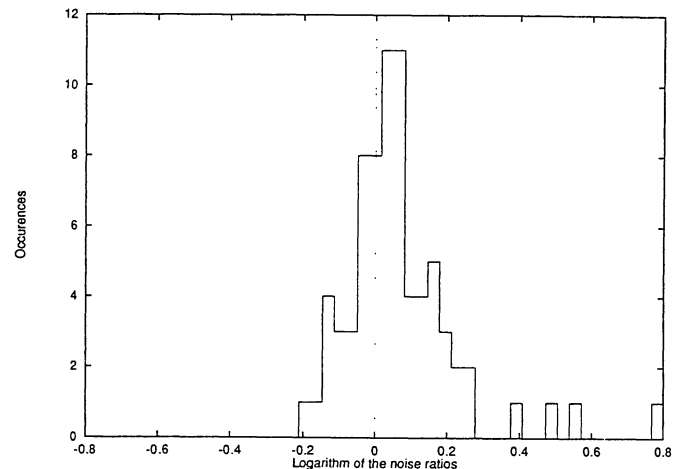

Fig. 7. Histogram of the logarithm of the ratios of the noise values determined by methods (a) and (b). The standard deviation associated to this distribution is 0.16

5.3. Noise inhomogeneity

One of the first obvious properties is the dispersion between the different subapertures. Figure 8 illustrates such a dispersion. The graph has been computed from a slope set of 1024 frames covering 5.12 seconds. The correlation time of the spot fluctuations being between 60 and 70 ms, it remains small compared to the length of the record. Hence, the non-uniformity does not come from a lack of averaging. The heterogeneous structure does exist permanently and can be found on several sets of data taken in the same conditions.

Possible causes for this dispersion are numerous. The inner subapertures, given their smaller area, are systemat-

ically noisier than the others. A local turbulence internal to the dome or to the telescope for thermal exchange reasons may produce localized turbulent eddies on the pupil, making some spots asymmetrical and wandering in particular directions, hence leading to different noise variances. Finally, a number of factors could affect the symmetry of the spot images, such as the residual static aberrations of the primary mirror and of the sensing optical channel, the non-uniformity of the detector and of the intensifier point-spread function, the aberrations of the micro-lenses, the shape of the subapertures (diffraction effects). Unfortunately, the raw images coming from the detector of the WFS are not stored in ComeOnPlus. It is then difficult to establish a link between these fluctuations on the noise values and the shape of the spots. The information contained in the centroid fluctuations is not sufficient to properly interpret this.
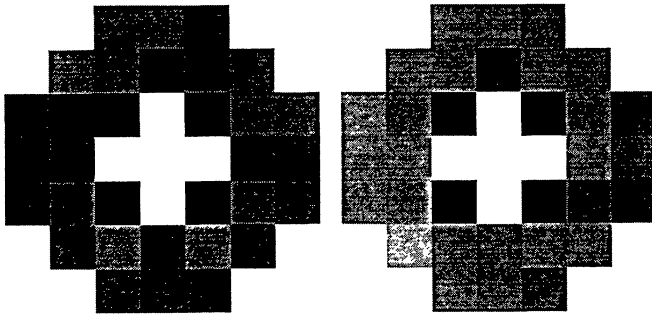

Fig. 8. Each "pixel" represents the localisation of a subaperture of the Hartmann and the grey level the noise variance in it. The left picture stands for the x directions, the right one the y. The noise variance ranges from 0.011 to 0.038 arcsec^2
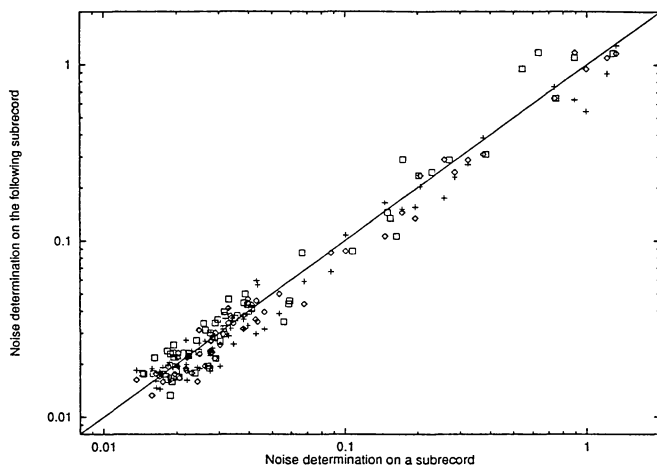

Fig. 9. Noise determination on one subrecord of 1024 frames versus the noise determination on the following subrecord

The dispersion pattern does not change when the noise is evaluated in different parts of a unique long slope set.

Figure 9 is obtained from a slope set of 8192 frames, recorded at a 200 Hz sampling rate. This represents a total time window of 41 s. The set has been subdivided into 8 subsets of 1024 frames each, and the calculus of the noise variance has been done on each of these subsets. Here it is proposed to show that the inhomogeneities found with method (b) are significant, and not due to random fluctuations. For this, the noise results obtained on one subset are compared with the ones from the following subset. The results are plotted in Fig. 9. Numbering the subsets from 1 to 8, the differents plots represent the 64 noise values of subset 3 versus subset 1, 7 versus 4 and 8 versus 5. The dispersion along the full correlation line proves the dispersion of the noise over the pupil. The dispersion in a perpendicular direction to this line is due both to the limited accuracy of the method, and to the noise variation -even if weak- between the different subrecords. One can notice that this last dispersion is much weaker than the noise inhomogeneities.

We have now a good knowledge of the performance and the limitations of the noise determination method. This was needed, as the uncertainties on the noise level will be used as inputs to evaluate the performance of the optimization algorithm in Sect. 7.

6. The modes

The optimization process works in a manner independent of the set of modes which is chosen. Hence, this choice is not coupled with the optimization algorithm and remains arbitrary. However it is well known that some modes are better suited for atmopheric compensation than others (Wang & Markey 1978; Roddier et al. 1991) and moreover the mode set is constrained by the AO system configuration.

Hence, the choice of the modes set for the ComeOnPlus system is not arbitrary. The detailed computation procedure is beyond of the scope of this article ; only the general properties are described.

Modes such as Zernike polynomials (Noll 1976) or the modes obtained by the Karhunen-Loeve decomposition of the turbulence process (Wang & Markey 1978) are never used in real-time control. The modes are defined as a set of voltages to be applied to the mirror actuators. They are chosen to be orthogonal between each other in order that $\int_{\mathrm{Pupil}} m_i(x,y)\, m_j(x,y)\, \mathrm{d}x\, \mathrm{d}y = \delta_{ij}$. This property allows the addition of the errors on each mode to obtain the total error. The modes are chosen to be statistically uncorrelated between each other. The computation is theoretical and assumes a Kolmogorov-type turbulence. This property leads to a mode set where the correction of one mode leads to the minimization of the global phase variance due to this mode. It is a kind of Karhunen-Loeve decomposition.

Some modes may happen to cause problems because the WFS is blind to them. Two well-known examples of

such modes are the piston mode and the waffle mode (Wild et al. 1994a, b). In fact, four modes belonging to this class are identified in the case of ComeOnPlus and suppressed from the correction.

Finally, the set of modes has to contain pure tip and tilt, to be corrected by the dedicated fast steering mirror. The deformable mirror is also able to produce the tip-tilt modes, but firstly their maximum amplitude is insufficient for atmospheric compensation and secondly they are redundant with the steering mirror. Hence, these tip and tilt modes of the deformable mirror are identified and also suppressed from the correction.

The total number of degrees of freedom of the ComeOnPlus system is 54 (52 actuators plus 2 given by the steering mirror), but only 48 degrees are actually controlled.

7. Modal control optimization

Once the noise determined it becomes possible to proceed, by using the general method of modal control optimization fully described in Paper I. We briefly recall here this optimization scheme and deduce the uncertainties on the optimum bandwidths and residual phase errors.

7.1. Optimization of the modal control

The wavefront is decomposed over a basis of spatial modes. Because each mode behaves differently, a particular correction bandwidth is associated with each one. This bandwidth is controlled by a coefficient called *modal gain*. The problem consists of finding the optimum gain for a given mode, knowing that the modes are not cross-coupled and that the optimum value leads to the minimum phase error on this mode (Gendron & Léna 1994a). The algorithm differentiates the error on the mode with respect to the modal gain and searches for a null value.

The input parameters required to compute the residual error (or its derivative) are the noise variance (or noise level) and the power spectral density of the mode fluctuations.

The system transfer function $h_{ol}(f, g_i)$ is known, at least in the ComeOnPlus case, it is accurately modelized. The sampling frequency and the unavoidable time lag between measurement and control are known and included in the mode transfer function.

The turbulence leads to a particular, possibly time-dependent, temporal power spectrum of the mode. To estimate it and use it as an input parameter in the optimization of the modal gains, it is necessary to record, before closing the servo-loop, an uncorrected slope set. This same recording provides (through method (b) described above) the noise variance estimate, including both the turbulence and the system noise.

After extracting these parameters, the residual error on one mode is computed by (see Paper I)

$$\epsilon_0(g) = \int H_{cor}(f,g).(T(f)+B(f)-b_0)\mathrm{d}f + b_0.\int H_n(f,g)\mathrm{d}f \quad (7)$$

The above equation stands for one particular mode i, and all the variables should be indexed with this subscript. It will be omitted below for the sake of brevity.

$\epsilon_0(g)$ is the residual phase error on the mode varying in terms of the modal gain g. $H_{cor}(f,g)$ is the correction transfer function of the system, depending on the frequency f and the modal gain g. $T(f)$ is the power spectral density of the mode fluctuations due only to the turbulence and $B(f)$ is the power spectral density of the noise propagated on the mode. b_0 is its average level, i.e. $b_0 = 2/F_e \int_0^{F_e/2} B(f)\,\mathrm{d}f$. For each mode, the residual error is the sum of the residual error produced by the finite correction bandwidth plus the error due to the noise (Eq. (7)). As these quantities vary in opposite sense with frequency, the sum may reach a minimum. In Paper I, it was shown that the rms uncertainty on this estimate of the residual error is $\frac{F_e}{2} b_0/\sqrt{K}$ where $2K$ is the number of frames used in the slope set.

The parameter searched for is the modal gain g, or the associated correction bandwidth ν since there is a one-to-one relation between them. In the following we refer to the latter, which has an obvious physical interpretation.

7.2. Uncertainty in the determination of the optimum bandwidth and influence on the residual error

Despite the precautions discussed above, the b_0 estimate may suffer from experimental errors, which in turn affect the uncertainty on the residual phase error. The purpose of what follows is to estimate the uncertainty on the optimum correction bandwidth ν and derive its effect on the optimized residual phase error. Let define $\epsilon(\nu)$ as the residual error computed with a noise level b instead of b_0. We have

$$\epsilon(\nu) - \epsilon_0(\nu) = -(b-b_0).\int (H_{cor}(f,\nu) - H_n(f,\nu))\,\mathrm{d}f \quad (8)$$

The quantity $\frac{F_e}{2}\alpha(\nu) = \int(H_{cor} - H_n)$ depends on the system only. Figure 10 shows some plots of $\alpha(\nu)$ versus ν for the sampling frequencies 100, 50 and 25 Hz. It shows that the variation of $\alpha(\nu)$ is small, and hence $\epsilon(\nu)-\epsilon_0(\nu) \approx -\frac{F_e}{2}(b-b_0)$ is nearly independent of ν.

Let define ν_0 as the actual optimum value, and expand $\epsilon(\nu)$ near ν_0. It comes

$$\epsilon(\nu) = \epsilon_0(\nu_0) + \frac{\epsilon_0''(\nu_0)}{2}.(\nu - \nu_0)^2 - (b-b_0).\alpha(\nu) \quad (9)$$
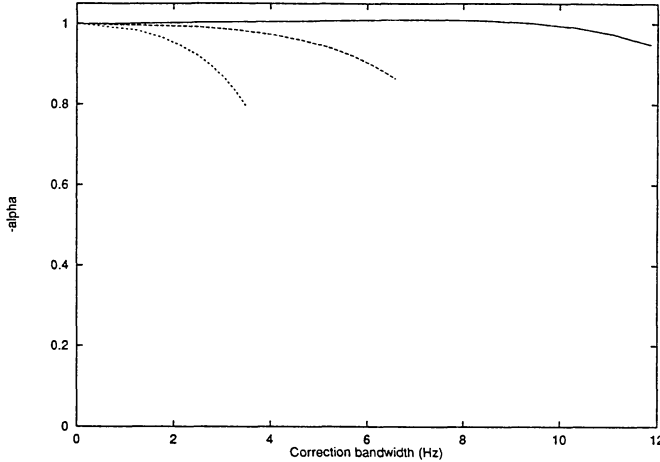
Fig. 10. Values of $\alpha(\nu)$ in terms of the correction bandwidth ν. The plain line corresponds to a sampling frequency of 100 Hz, the dashed line to 50 Hz and the dotted one to 25 Hz. For each sampling frequency, the curves are plotted up to the correction bandwidth leading to an unstable close loop. The function $\alpha(\nu)$ is nearly a constant and this approximation becomes better as the sampling frequency grows

In order to find the location of the minimum, expression (9) is differentiated with respect to ν. This leads to the wrong optimum value ν_w

$$\nu_w = \nu_0 + \frac{(b-b_0)\,\alpha'(\nu)}{\epsilon_0''(\nu_0)}\,\frac{F_e}{2} \qquad (10)$$

Now, in order to compute the *actual residual error* when using the *wrong* optimum value ν_w given by Eq. (10), we replace Eq. (10) in (9) with $b = b_0$. It gives

$$\frac{\epsilon_0(\nu_w) - \epsilon_0(\nu_0)}{\epsilon_0(\nu_0)} = \frac{1}{2}(b-b_0)^2 \frac{1}{\epsilon_0(\nu_0).\epsilon_0''(\nu_0)}\,\alpha'^2(\nu)\left(\frac{F_e}{2}\right)^2 \qquad (11)$$

Knowing we only need a rough estimate, a simple model has been used for the evaluation of $\epsilon_0(\nu_0).\epsilon_0''(\nu_0)$. The calculus is given in Appendix. One gets the expected quantity

$$\epsilon(\nu_0).\epsilon''(\nu_0) = b_0^2\,\frac{u^2}{u-1} \qquad (12)$$

where u is the slope of the high frequency behavior of the spectrum (in f^{-u}).

When replaced in Eq. (11), it gives

$$\frac{\epsilon_0(\nu_w) - \epsilon_0(\nu_0)}{\epsilon_0(\nu_0)} = \frac{1}{2}\frac{u-1}{u^2}\frac{(b-b_0)^2}{b_0^2}\,\alpha'^2(\nu)\left(\frac{F_e}{2}\right)^2 \qquad (13)$$

Making the assumption that $\frac{F_e}{2}\alpha'(\nu) < 1$ is a reasonable value (common values are $\alpha'(\nu) \approx 0$ to 0.5 and $\alpha'(\nu) = 2$ is an extreme case) and taking $u \approx 3$ leads to

$$\frac{\epsilon_0(\nu_w) - \epsilon_0(\nu_0)}{\epsilon_0(\nu_0)} < 0.11\left(\frac{b-b_0}{b_0}\right)^2 \qquad (14)$$

and to

$$\frac{\nu_w - \nu_0}{\nu_0} = -0.33\,\frac{b-b_0}{b_0} \qquad (15)$$

As a numerical application, a relative error of 0.33 on the noise level -which is already a large value- gives a relative error of 0.10 on the optimum bandwidth ν_0. The error on the calculated residual error is nearly the same than for the noise, i.e. 0.33 times the noise variance. The point is that the *actual* residual error only differs of about 1% from the expected value (4% in the really worst case). It means that it is possible to correctly tune the modal gain and to reach the optimum point with a good accuracy, without being able to determine the value of the actual residual error at this optimum with the same accuracy.

Readers of this article should not be alarmed by negative variances. Although these are clearly non physical, such things may happen since it is often required to subtract variances of given quantities from each others. In particular, when dealing with extremely noisy data the uncertainty on the noise estimate, even if not so large, may happen to be larger than the turbulent signal itself. We would like to insist on the fact that finding an absurd result for the value of the residual error -typically a negative value- does not mean that the value of the optimum bandwidth is wrong.

As an example, we propose to show the behavior of the optimum bandwidth when the noise is not properly determined. For this, the optimization process will be applied on the same set of data while giving as input different values for the noise level b, ranging from 0 to $2\,b_0$. Figure 11 shows the residual error versus the correction bandwidth for a coma-like mode, but similar results apply for any other mode. The input data come from experimental data, and the conditions are summarized in the caption. Although the entered noise value b varies over a large interval the position of the minimum changes slightly. Moreover the curve is very flat near ν_0 and the changes on the actual minimum value have only a tiny effect on the actual residual error value. For very large values of the noise, the residual error goes negative: although meaningless, this does not prevent the search for the minimum and gives a good value for the optimum.

8. Results

This section aims to present some results of the optimization in various situations. The results are entirely linked to the ComeOnPlus AO system and its environment. First a description of the experimental shape of the residual phase error versus ν_0 is given, then the robustness of the optimization process is discussed. Finally, we give an overview of the system correction capabilities for different stellar magnitudes.

Magnitudes of the reference source used in the following paragraphs are always given for the V band ($\lambda = 550$ nm).
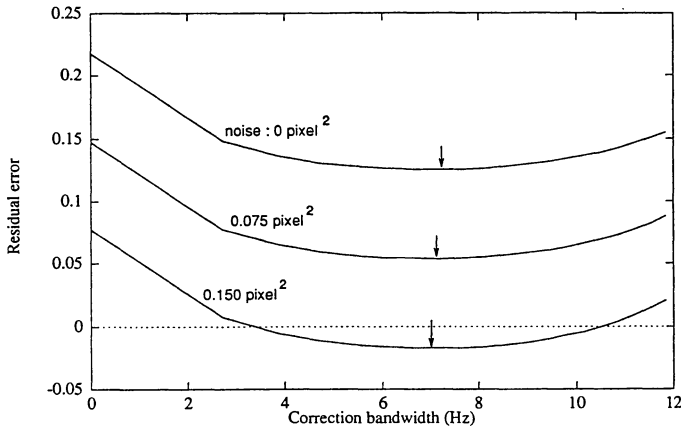
Fig. 11. Residual phase error (arbitrary units) versus the correction bandwidth for a coma-like mode. The parameter for each curve is the noise level b_0 (see Eq. 7). The true value is a noise of $b_0 = 0.075$ pixel^2 on the centroid determination. The optimum value of the correction bandwidth only varies from 7 to 7.5 Hz. The conditions were a r_0 of 10.1 cm, a correlation time of 80 ms. The reference star magnitude is $m_V = 11.1$, the EBCCD was used

8.1. Residual error versus the correction bandwidth

As exemplified in Fig 11, the residual phase error versus the correction bandwidth $\epsilon(\nu)$ is always a smoothly-varying function despite the jerky aspect of the turbulence spectra. This is because each point of $\epsilon(\nu)$ depends on the entire turbulence spectrum. Hence cases with several minima have never been detected. The most complex cases have a maximum before reaching the minimum searched for, but this only happens in exceptional occasions when the turbulence is extremely fast.

8.2. Robustness of the optimization

We have already proven that the noise estimation and the way it enters into the optimization process acts as a second order effect in the accuracy of the results. We now propose to examine the influence of the turbulence parameters.

Two points have to be investigated. The first one is the robustness of the optimization process. Let assume the observing conditions to be constant, i.e. the key parameters such as the coherence length r_0 and time τ_0 are stable and the shape of the modes spectra do not change. Even with this unphysical conditions the optimization may give varying results simply because it is based on a particular sequence taken before closing the loop, which is a single realization of the phenomenon.

The second point is to evaluate the influence of the non-stationnarity of the turbulence, since the optimum parameters are deduced from a sequence taken a given

instant *before* closing the loop and the atmosphere state may evolve during the observation.

Our concern here is to analyse the first point but unfortunately both aspects are systematically mixed when dealing with experimental data. A good test to study the robustness is to perform the optimization on several sequences of turbulence taken with identical conditions and at very close intervals in time. A typical number of frames needed for an optimization is 1024. As the system can record slope sets of 8192 frames, it is possible to subdivise one of them in 8 subrecords of 1024 frames and to look how the optimization behaves on each. In order to limit the number of plots, we choose to plot the correction bandwidths obtained for a subrecord versus the values averaged over the 8 subrecords, and superimpose all the results (Figs. 12 and 13). Slopes sets have been selected to cover different cases of observing conditions.

The first example will be called (A) below and is plotted in Fig. 12. It is a case with a good signal-to-noise ratio. The second one, called (B) (Fig. 13), is taken on a reference star of magnitude $m_V = 12.1$, leading to a bad signal-to-noise ratio. One may notice that in this last case, the correlation time of the fluctuations directed along one axis is 100 ms when it is 210 ms for the fluctuations directed along the perpendicular axis. The telescope inclination (29 degrees from the zenith) is responsible, together with the wind direction, for the anisotropy of these temporal characteristics, as the pupil projected on a particular turbulent layer no longer presents circular symmetry.

Table 2. Values of the Fried's parameter r_0 (cm), given at $\lambda = 500$ nm, and of the correlation time along the x or y directions. The eight values correspond to eight subrecords of 1024 frames taken in a global slope set of 8192 frames

	1	2	3	4	5	6	7	8
(A)								
r_0	8.2	8.2	9.3	8.5	7.6	7.1	6.6	8.2
$\tau_{x/y}$	55	55	53	55	53	53	58	58
(B)								
r_0	10.7	10.7	10.8	9.9	10.3	10.3	10.3	9.9
τ_x	260	155	230	200	170	200	230	185
τ_y	85	100	85	90	90	100	105	90

Table 2 gives the r_0 and τ_0 values measured during the eight subrecords. The values of r_0 are deduced from the fluctuations of the angle of arrival σ_α^2 according to the formula given by Sante (1975).

$$\sigma_\alpha^2 = 0.17 \lambda^2 \, d^{-1/3} r_0^{-5/3} \left[1 - 1.49 \left(\frac{D}{L_0} \right)^{1/3} \right] \quad (16)$$

The term between brackets is the attenuation term due to the outer scale of turbulence L_0. Two values of σ_α^2 (σ_α^2

for a subaperture and σ_α^2 for the entire telescope pupil) provide two equations allowing to solve for r_0 and L_0.[1]

The values of the wavefront correlation time τ_0 are the half width at half maximum of the autocorrelation function of the wavefront local slopes after removing tip and tilt.

Although the differents subrecords have been taken very near in time, the atmospheric conditions did fluctuate, as shown on Table 2 (the error on each r_0 is less than 0.5 cm). However, the time interval between the beginning of the subrecords is 5.12 seconds in the case (A) and 14.6 seconds for (B). These are very short time scales, and it will be considered that these fluctuations are due to the ramdom characteristics of the process, more than actual changes in the turbulence key parameters.

Fig. 13. Record (B). Optimum correction bandwidths computed on 8 successive slope sets of 14.6 seconds long, versus the averaged values. The conditions are a $r_0(500\text{ nm}) = 10.1$ cm, a correlation time of 100 ms and 210 ms depending on the fluctuations direction. The sampling frequency is 70 Hz. The star magnitude is $m_V = 12.1$

Fig. 12. Record (A). Optimum correction bandwidth computed on 8 slope sets of 5.1 seconds long, versus the averaged values. The conditions are a $r_0(500\text{ nm}) = 8.1$ cm, a correlation time of 55 ms. The sampling frequency is 200 Hz. The observed object is Titan, with a visual magnitude $m_V = 8.3$

The dispersion around the full correlation line does not appear to be so small. However, combining Eqs. (9), (21) and (22) proves that

$$\frac{\epsilon_0(\nu) - \epsilon_0(\nu_0)}{\epsilon_0(\nu_0)} \approx \left(\frac{\nu - \nu_0}{\nu_0}\right)^2 \qquad (17)$$

Figure 14 exhibits the histogram of the values of $\frac{\epsilon_0(\nu) - \epsilon_0(\nu_0)}{\epsilon_0(\nu_0)}$ for the two previous cases (Figs. 12 and 13). It shows that for over 96% of the cases the relative accuracy is better than 0.04, and is better than 0.01 for 70% of the cases.

The relative precision increases with the signal to noise ratio. The dispersion is due to the combination of the

Fig. 14. Histogram of the values of $\frac{\epsilon_0(\nu) - \epsilon_0(\nu_0)}{\epsilon_0(\nu_0)}$ for the cases (A) (plain line) and (B) (dashed line) described above

uncertainty on the noise determination, on the random character of the atmosphere and for a minor part to the non-stationnarity. Also in the case (B) the time interval between the subrecords is longer, possibly enlarging the dispersion. Even with this, the accuracy on the residual phase error is most of the time of the order of 1%.

8.3. Stars brighter than $m_V = 7$

This is a high flux case. The WFS used is the Reticon array. The sampling rate is 200 Hz, and the delay between the end of the integration time of the WFS and the moment the control is applied on the mirror is 2 ms. In such cases, the signal-to-noise is good enough to allow the full

---

[1]This method leads also to an independent determination of L_0. With the above r_0 values we get $L_0 \simeq 13$ m for case (A) and $L_0 \simeq 75$ m for (B). Therefore, the system provides a tool to follow the outer scale evolution, although the method is sensitive to telescope tracking errors.
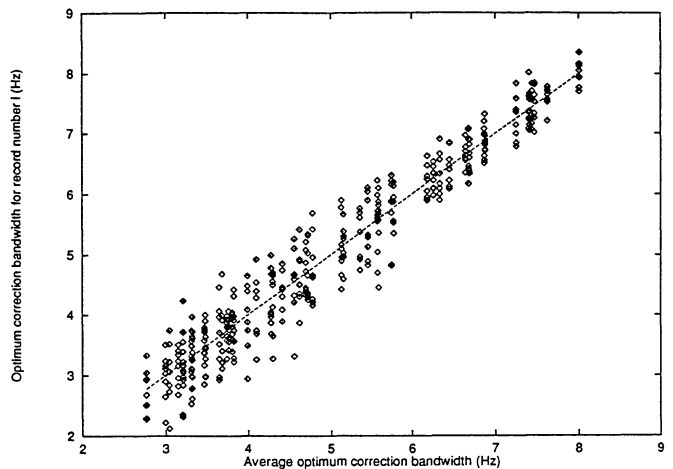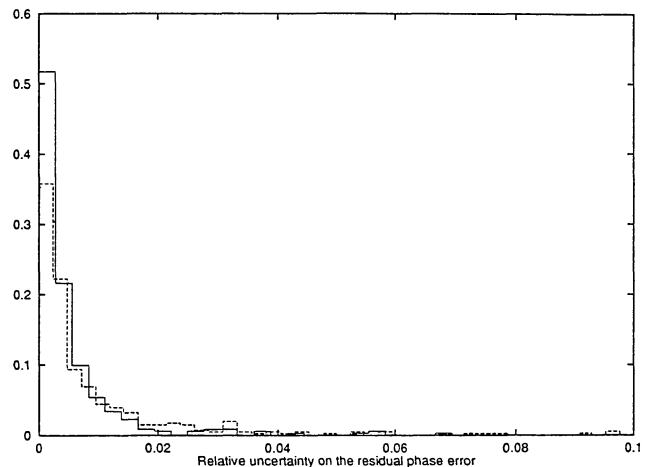
control of the modes and the maximum gain can be applied to all modes.

8.4. Stars with $7 \leq m_V \leq 9$

It is a regime where some noise appears on the measurements. An example of such a case has already been presented in Fig. 12. The first modes can always be fully controlled with the maximum bandwidth, but the high order ones begin to be filtered.
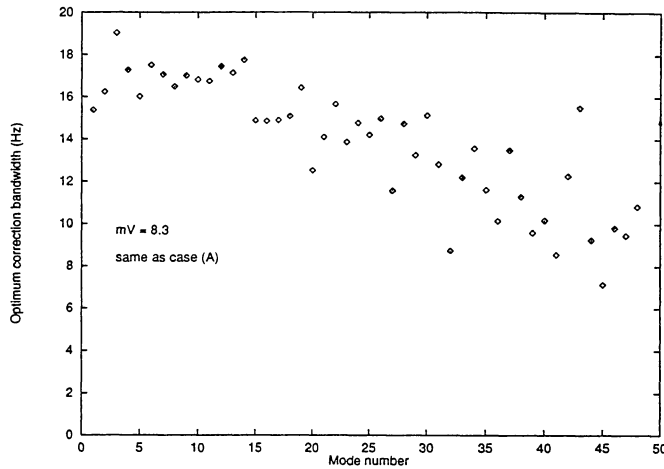

Fig. 15. Optimum correction bandwidth computed on a slope set record of 1024 frames long. The conditions are a $r_0(500$ nm$) = 9.6$ cm, a correlation time of 50 ms, a $m_V = 8.3$, a diameter of 0.8 arcsec. The sampling frequency is 200 Hz. Data recorded on Sept. 1st 1993, at 5h29 UT

The two cases presented here (Figs. 15/16 and 17/18) are taken on the same reference object (Titan), with the same WFS and in the same conditions but two nights apart. The correction bandwidths are the same for the low-order modes but become slightly different for higher-order ones. Figures 15 and 17 show the optimum correction bandwidth for each mode, and Figs. 16 and 18 are the associated plots showing the correction efficiency: the value plotted is the ratio between the corrected and uncorrected phase error of each individual mode. This ratio tends towards 1 as the mode order grows, showing that the correction becomes less efficient for high spatial frequencies. This is due to the decrease in the mode signal to noise ratios, along with the increase of their evolution speed.

8.5. Stars with $10 \leq m_V \leq 11$

The object selected here is a star of $m_V = 10.6$. The real magnitude of the star (SAO 167022) was $m_V = 7.5$, but it has been reduced to $m_V = 10.6$ with a neutral density filter since it was used during an astronomical observing run as a point spread function calibration for another source of magnitude 10.5. The conditions of seeing are good. The
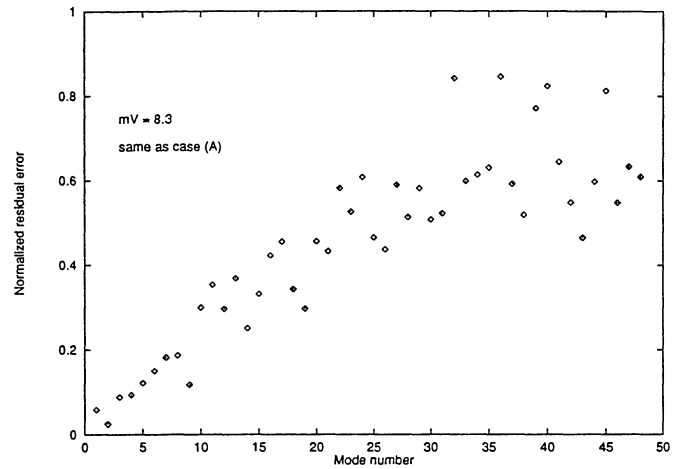

Fig. 16. Ratio between the phase variance after correction and before, corresponding to Fig. 15. The first modes are well corrected while higher order modes are not. In this case only 25 modes are corrected better that 50%. It must be noticed that contrary to the optimum bandwidth values, the normalized residual error determination is not accurate, except for good correction cases
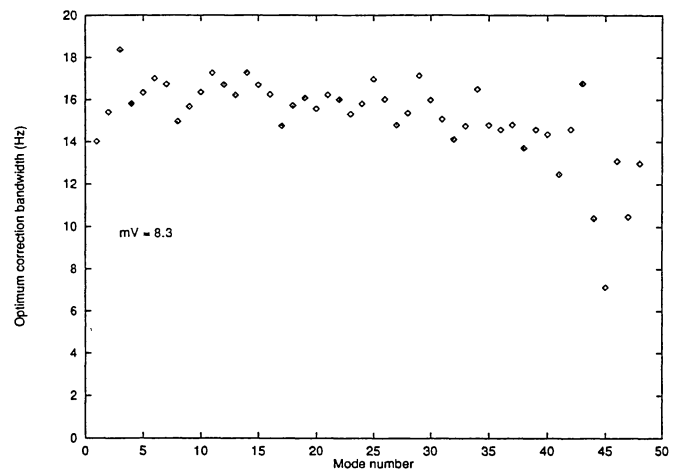

Fig. 17. Optimum correction bandwidth computed on a 1024 frames long slope set record. The conditions are a $r_0(500$ nm$) = 8.1$ cm, a correlation time of 55 ms, $m_V = 8.3$. The sampling frequency is 200 Hz. Those data have been recorded on Sept. 3st 1993, at 07h17 UT

optimum bandwidths and correction efficiency are shown in Figs. 19 and 20. It is interesting to notice than despite the magnitude of 10.6, the normalized residual errors are much better than for the previous cases. Nearly all the modes are corrected better than 50%. The sampling frequency was 200 Hz, as in the previous cases. The difference stands in the seeing conditions: the r_0 value is 13.3 cm, but the correlation time is $\tau \approx 160$ ms. This is approximately 3 times larger than in the previous paragraph (8.4).
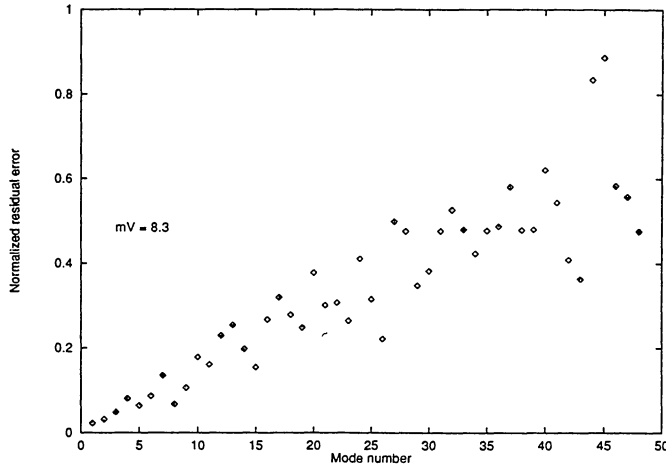
Fig. 18. Ratio between the phase variance after correction and before, corresponding to Fig. 17. The correction efficiency decreases with the mode order. Only 42 modes are corrected better than 50%
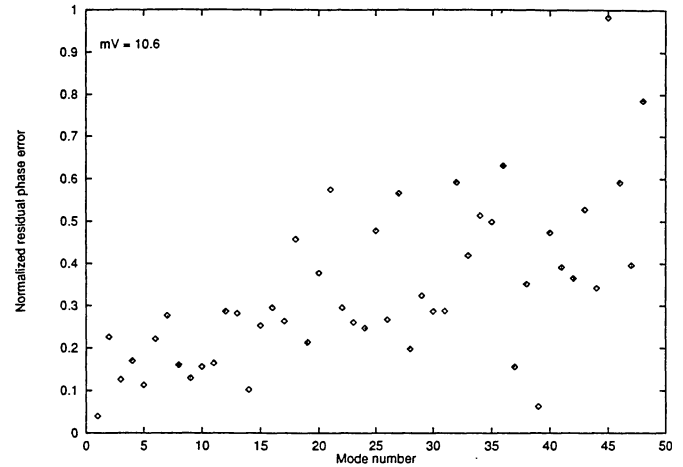

Fig. 20. Ratio between the phase variance after correction and before, corresponding to Fig. 19. There are 41 modes corrected better than 50%
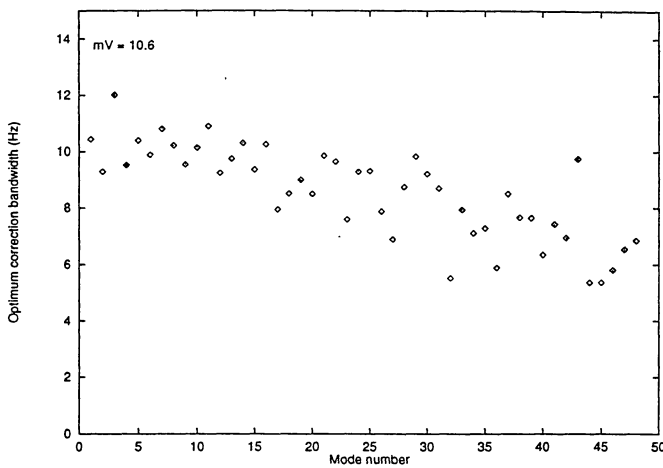

Fig. 19. Optimum correction bandwidth computed on a 1024 frames long slope set record. The conditions are a $r_0(500$ nm$) = 13.3$ cm, a correlation time of 160 ms, an equivalent magnitude of $m_V = 10.6$. The sampling frequency is 200 Hz. The data have been recorded on Oct. 27th 1993, at 06h27 UT

In Fig. 22, the strong uncertainty on the residual phase error really becomes a nuisance. Only the two first modes have a signal to noise ratio greater than 2: the modes 3 to 10 have signal to noise ratios comprised between 0.8 and 0.08, and most of the other modes are below 0.1. Hence, an error of 5% on the noise level makes 50% error on the normalized residual error. The data have been plotted between 0 and 1, but 3 values were found to be greater than 1, and 7 found to be negative. The plot is simply indicative. It allows one to guess the global shape of the curve, but one cannot trust the individual values: a theoretical analysis would give better results. However, despite the bad quality of these values, it is recalled that the uncertainty on the optimum bandwidth is less than 5%.

8.7. Stars with $m_V \approx 14$

The correction capabilities at this low flux level are extremely dependent on the turbulence conditions. The values of r_0 and the correlation time are the determining factors.

8.8. Special cases

8.8.1. Fast turbulence

A particular case of correction applies when the turbulence conditions are exceptionnaly fast. A correlation time of the order of magnitude of the sampling frequency is needed. In such conditions, the optimization will lead to tuning the correction bandwidth primarily because of the turbulence speed, rather than because of the noise level. When the correlation time of the mode, although short, is sufficiently long to be corrected by the system, a large correction bandwidth is applied. When the mode correlation time is shorter than the integration period plus the
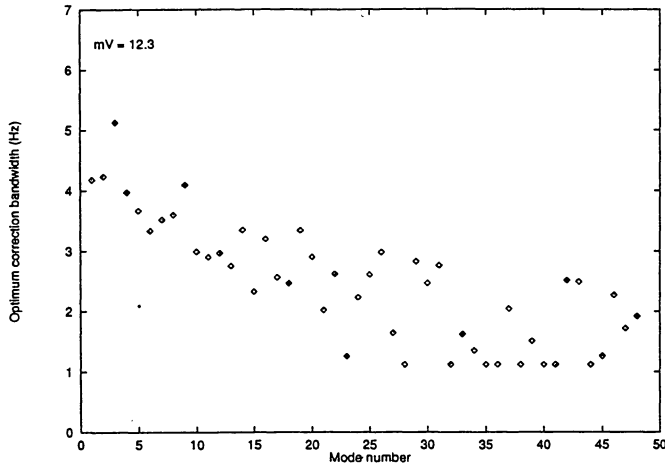
8.6. Stars with $12 \leq m_V \leq 13$

The first example is taken on a $m_V = 12.3$ magnitude star. The sampling frequency used is 100 Hz. Due to the good seeing conditions ($r_0 = 16.6$ cm at 500 nm) the signal to noise ratios are poor, leading to low correction bandwidths. This is enhanced by the slowness of the turbulence: ($\tau \approx 100$ to 160 ms). Again, the inclination of the telescope (more than 30 degrees from the zenith) makes the turbulence anisotropic. Figure 21 shows the optimum bandwidths and Fig. 22 the normalized residual errors.

Fig. 21. Optimum correction bandwidths, in Hz, versus the mode number. The seeing conditions are good and the evolution speed is pretty slow. $r_0 = 16.6$ cm at 500 nm and $\tau \approx 100$ to 160 ms. This tends to produce low correction bandwidths, here between 1 and 5 Hz (the minimum value of 1.12 Hz was imposed by the software)
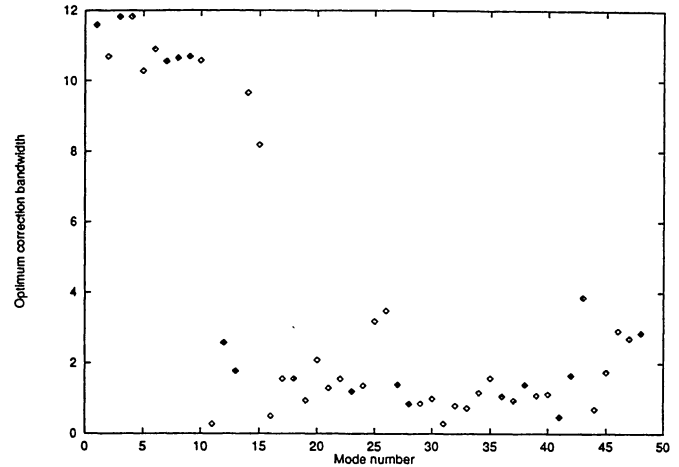

Fig. 23. Optimum correction bandwidth in terms of the mode number. The sampling frequency is 100 Hz. The r_0 is 8.5 cm, and the correlation time of the angle of arrival is 30 ms. The correlation time of the tilt is 150 ms, it is 45 to 35 ms for the defocus and astigmatism-like modes, and 20 to 5 ms for the higher modes
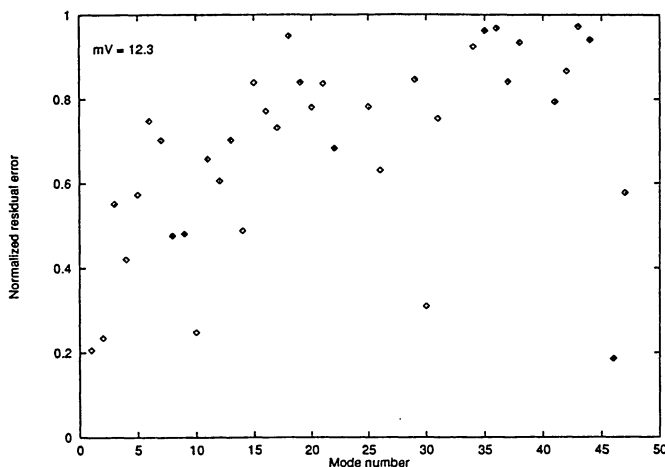

Fig. 22. Ratio between the phase variance after correction and before, corresponding to Fig. 21

lence produced by a single layer moving along at a speed of 14 m.s^{-1}.

8.8.2. Fan problem

Telescopes are usually designed to offer pointing accuracies better than the seeing conditions. During the Come-OnPlus observations in December 1993, an unexpected pointing error problem, until then hidden by the seeing, was discovered, causing the modal control algorithm to reduce the tilt correction bandwidth to an abnormal value far below higher order modes. After investigation, the cause was found to be a vibration produced by a cooling fan at a frequency of 25 Hz, of about 0.3″ peak to peak. Given the sampling frequency used on the WFS, this vibration was in a zone of the system correction transfer function where it was amplified rather than corrected, unless the correction bandwidth was be reduced.

Firstly, this proves the independence of the modal control optimization in terms of the perturbation to correct. Secondly, it shows that the use of an AO system does not always relax the telescope stability requirements, but may impose some new constraints on it.

9. Number of corrected modes in terms of the star magnitude

We propose here to sum up the conclusions of the previous section. Unfortunately there is no synthetic parameter characterising the correction. The residual phase variance strongly depends on the uncorrected variance; their ratio depends on the correlation time. In order to characterize the correction efficiency in a modal way, we chose to

time delay, the mode is completely supressed. This leads to situations where the modal gains behave in a binary way. The low-order modes nearly have the maximum correction bandwidth while the others, higher order modes, are not controled (0 Hz bandwidth).

In the general case, the correction bandwidth difference between low and high order modes increases with the speed of the turbulence, and the gap becomes a maximum when the correlation time of the highest modes reaches the sampling time. Figure 23 shows an example of such a case. After more thorough study, this case has been shown (Gendron & Léna 1994b) to be due to a turbu-

plot the number of corrected modes in terms of the reference star magnitude. Knowing that no mode is completely corrected or uncorrected (see Figs. 16, 18, 20 and 22) we arbitrary decided that a mode is corrected or not according to the ratio between the corrected phase variance and the uncorrected one. It is considered as corrected when this ratio is below a given threshold. Figure 24 shows the number of corrected modes in terms of the magnitude, for a threshold of 0.20. Figure 25 shows the same set of data, with a threshold of 0.50.
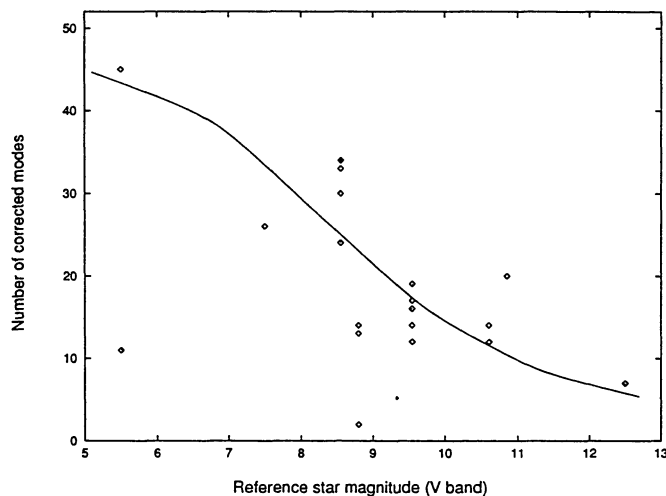

Fig. 24. Number of modes on which the phase error after correction is less than 0.20 times the initial phase error, versus the magnitude of the reference star
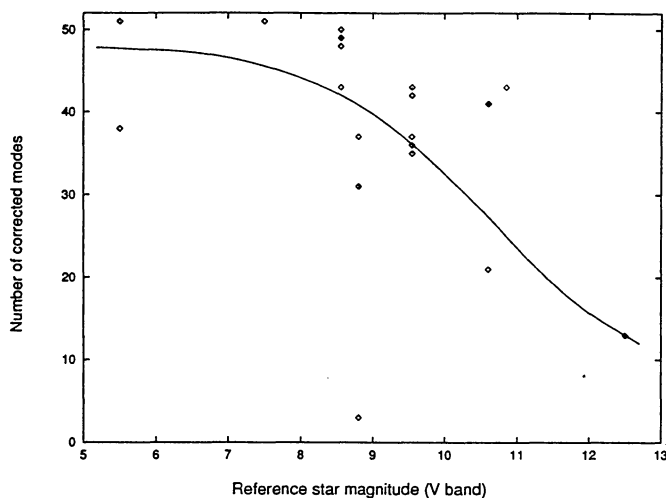

Fig. 25. Number of modes on which the phase error after correction is less than 0.50 times the initial phase error, versus the magnitude of the reference star

The points spread widely around the average value. The main reason for this dispersion is not the lack of accuracy of the determination method. As a matter of fact these deviations are significant. In some cases they depend on the reference object observed, but for most of them

they are characteristic of different turbulence conditions and atmospheric structure. The parameters r_0 and τ_0 do not suffice to entirely define the state of the turbulence.

10. Conclusion

We studied the behavior of the modal control optimization process using the data collected with the astronomical AO system ComeOnPlus and demonstrated its efficiency in terms of minimizing the overall phase variance, taking into account any specific configuration of the observing conditions.

A key point for a correct computation of the optimization is a good knowledge of the WFS noise level. It has been shown that the method used to derive it allows one to obtain an relative accuracy of about 10% on the averaged noise variance, and shows evidence of noise inhomogeneities between subapertures. This last point is of importance since the modes having a large value in front of the noisiest subapertures will be primarily affected.

The data from ComeOnPlus also allowed us to demonstrate that the turbulence itself may be spatially and temporally inhomogeneous over the pupil.

The impact on the optimization process of the inaccuracies in the noise measurement has been studied, as well as the robustness of the optimization. In most of the cases the minimum of the phase residual error is reached with a relative error of 1% which is small, given the error bars on the noise determination and the non-stationarity of the turbulence.

Different cases have been illustrated, from magnitude $m_V = 8$ to 12, showing the correction to decrease progressively. For a given reference magnitude, the number of corrected modes may strongly vary from night to night because of the turbulence structure. This is the advantage of this optimization scheme, namely to be independent of any model and to rely only on the experimental data: it really allows the adaption of the correction to any situation. The magnitude scale used here is totally dependent on the ComeOnPlus system: e.g. increasing the quantum efficiency of the WFS photocathode by a factor of 2 would shift all the magnitudes.

One could object that using different gains for each mode is not always useful. Many cases exist, mainly when the correction is good, where the modal gains spread weakly around a mean value and where all the gains could be replaced by their average, hence leading to the classical zonal control. The point is that one does not know that this is appropriate as long as the optimization algorithm has not been applied. And once it has been applied there is no argument for using the average gain value rather than the modal gains themselves.

As we took the ComeOnPlus system as an example, the case of an integral compensator with a gain has been studied here. Further improvements may lead to more complex compensators where several parameters per mode

are to be optimized, instead of one in the present case. However the principle remains the same, as long as the close loop transfer function can be modeled.

Another practical problem to solve is to decide how often the optimization scheme has to be applied. While integrating hours on a particular object, atmospheric conditions do vary. In such a case the optimization must be redone while the loop is closed. To obtain the required open loop set, one deduces it from a close loop one by adding to this latter the mirror deformation as seen by the WFS, i.e. the sequence of the mirror driving signals multiplied by the interaction matrix.

Having chosen the residual phase variance as the optimization indicator, there was no need to examine the images themselves, as they are provided by the camera associated with the AO system. Indeed, it is straightforward to deduce the image properties from a knowledge of the wavefront. On the other hand, users of AO work on images. In a forthcoming paper (Beuzit et al. 1994) a detailed analysis of observed astronomical images will be presented, when applying modal control optimization.

Appendix

We propose to evaluate $\epsilon_0(\nu_0).\epsilon_0''(\nu_0)$ (see notation in 7.2) knowing we only need a rough estimate. A very simple model is assumed: the turbulent spectrum is in $A.f^{-u}$, and the noise introduced is proportional to the correction bandwidth. Hence the residual error in terms of the correction bandwidth ν is

$$\epsilon(\nu) = b_0.\nu + A.\int_\nu^\infty f^{-u}\,\mathrm{d}f \qquad (18)$$

the derivative of which is

$$\epsilon'(\nu) = b_0 - A\nu^{-u} \qquad (19)$$

Hence, the optimum correction bandwidth ν_0 is obtained when the previous expression equals zero, or

$$\nu_0 = (A/b_0)^{1/u} \qquad (20)$$

The second derivative of $\epsilon(\nu)$ at ν_0 is

$$\epsilon''(\nu_0) = \frac{u\,b_0}{\nu_0} \qquad (21)$$

and the error at ν_0 is

$$\epsilon(\nu_0) = b_0.\nu_0\frac{u}{u-1} \qquad (22)$$

Finally, one gets the expected quantity

$$\epsilon(\nu_0).\epsilon''(\nu_0) = b_0^2\,\frac{u^2}{u-1} \qquad (23)$$

References

Beckers J.M. 1993, ARA&A 31, 13

Beuzit. J.L. et al. 1994, A&A, to be submitted

Conan J.M., Madec P.Y., Rousset G. 1992, 13th Sacramento Peak Summer Workshop on Real time and post-facto solar image correction

Cuby J.G., Richard J.C., Lemonier M. 1990a, Proc. SPIE 1237, 538

Cuby J.G., Kern P., Rigaut F., Rousset G. 1990b, Optique adaptative et VLT, eds. D. Alloin, P. Léna, Forum de l'Observatoire de Paris, 17

Ellerbroek B.L., Van Loan C., Pitsianis N.P., Plemmons R.J. 1994, JOSA 11, 2871

Gendron E., Cuby J.G., Rigaut F. et al. 1991, Proc. SPIE 1542

Gendron E. 1993, ed. F. Merkle, ICO Conf. on Active and Adaptive Optics, 187

Gendron E., Léna P. 1994a, A&A 291, 337

Gendron E., Léna P. 1994b, Experimental Astronomy, to be submitted

Hermann J. 1992, JOSA Comm. 9, 2257

Hubin N., Beuzit J.L., Gigan P. et al. 1992, Proc. SPIE 1780, 87

Léna P. 1990, Optique adaptative et VLT, eds. D. Alloin, P. Léna, Forum de l'Observatoire de Paris, 1

Léna P. 1994, Proc. SPIE 2201, 1099

Léna P. 1994b, eds. D. Alloin, J.-M. Mariotti, Adaptive optics for astronomy, NATO-ASI (Kluwer) 321

Madec P.-Y., Conan J.-M., Rousset G. 1992, ed. M.-H. Ulrich, ESO Conf. on Progress in Telescope and Instrumentation Technologies, 471

R.J. Noll, 1976, JOSA 66, 207

Rigaut F., Rousset G., Kern P. et al. 1991, A&A 250, 280

Roddier F., Northcott M., Graves J.E. 1991, PASP 103, 131

Roddier F., Northcott M., Graves J.E., McKenna D.L. 1993, JOSA 10, 957

Rousset G. 1992, private communication

Rousset G., Beuzit J.-L., Hubin N. et al. 1993, ed. F. Merkle, ICO Conf. on Active and Adaptive Optics, 65

Rousset G. Beuzit. J.L., Hubin N. et al. 1994, Proc. SPIE 2201, 1088

Sante R.L. 1975, Proc IEEE 63 No. 12, 1669

Wang J.Y., Markey J.K. 1978, JOSA 68, 78

Wild W., Kibblewhite E., Scor V. 1994a, Proc. SPIE 2201, 726

Wild W., Kibblewhite E., Shi F. et al. 1994b, Proc. SPIE 2201, 1121